Groundwater for Sustainable Development 12 (2021) 100531

Contents lists available at ScienceDirect

Groundwater for Sustainable Development

journal homepage: http://www.elsevier.com/locate/gsd

Research paper

A geomagnetic analysis for lineament detection and lithologic characterization impacting groundwater prospecting; a case study of Buffalo catchment, Eastern Cape, South Africa

Solomon T. Owolabi [a,*], Kakaba Madi [b], Ahmed Mukalazi Kalumba [a], Christopher Baiyegunhi [c]

[a] Department of Geology, Faculty of Science and Agriculture, University of Fort Hare, Private Bag X1314, Alice, 5700, Eastern Cape, South Africa
[b] School of Biological and Environmental Sciences, Faculty of Agriculture and Natural Sciences, University of Mpumalanga, Private X11283, Nelspruit, 1200, Mpumalanga, South Africa
[c] Department of Geology and Mining, University of Limpopo, Private Bag X1106, Sovenga, 0727, South Africa

ARTICLE INFO

Keywords:
Lithostratigraphic analysis
Hydrostratigraphic model
Macrostructures
Aeromagnetic analysis
Tectonic lines
Karoo supergroup

ABSTRACT

A lithostratigraphy analysis commonly adopted for subsurface structures exploration in oil prospecting is deployed for groundwater prognosis, due to the need to address the prevailing water shortage. In this study, the lithology characterization was based on a clustered approach of geomagnetic analysis, geomorphometric analysis, and sequence stratigraphy correlation across the Buffalo catchment, Eastern Cape, South Africa. The result showed the existence of a spatial correlation between the tectonic stress field and the surficial lineaments. Similarly, a significant azimuthal correlation (WNW-ESE) was found between surficial lineaments (203 m–6249 m), subsurface lineaments, and the neotectonic structures. The depth-slicing analysis enables the estimation of the depth of the tectonic stress field, at 382 m, 577 m, 913 m, 1.49 km, and 10.7 km in the subsurface. The sequence stratigraphy correlation based on borehole lithology data enables the identification of the fault system at the contact zones, heterolithic bedding, and the characterization of the hydrostratigraphic domain of the catchment. The study shows that Buffalo hydrostratigraphic structures are dominated by fracture networks, whereby the shallow groundwater resources are possibly hosted by the dolerite-host rock contact zones in the north of the Buffalo catchment. Specific recommendations concerning groundwater management are made to water and environment stakeholders considering the vulnerability of the shallow groundwater system to pollution in the permeable contact zones of dolerite-host rock. The study also recommends the adaptation of surficial lineaments as a morpho-tectonic aid and a hydrostratigraphic analysis tool. The clustered approach demonstrated in this study has important prospects for groundwater exploration in environments with similar geology.

1. Introduction

The understanding of geologic complexity has provided remarkable information on the variability of hydraulic properties and the zones of effective permeability that are significant to the flow of fluid in the subsurface. At a regional scale, fluid flow is channelled through large-scale structures of hydrostratigraphic units with significant permeability. For example, Ingebritsen and Manning (2003) demonstrated that the transmission of the metamorphic-fluid system and the continental crust degasification were controlled by large-scale crustal permeability at the continental margin. Bense and van Balen (2003) illustrated the effects of large-scale fault zones on the regional groundwater flux in the Roer Valley Rift System. Marker et al. (2015) presented a hydrostratigraphic cluster model based on sequential hydro-geophysical inversion for incorporating airborne electromagnetic data into the hydrological modeling process. Christensen et al. (2017) demonstrated a three-dimensional groundwater model using airborne electromagnetic data and lithology data. The geometry of geological structures was processed with the aid of the Bayesian geostatistical approach. Likewise, this study presents a clustered approach of geomagnetic analysis and lineament detection methods for the assessment of geologic structures in a complex geologic environment as a contribution to groundwater prospecting.

The major target zones in regional groundwater exploration are often

* Corresponding author. ;
E-mail address: solomonowolabi11@gmail.com (S.T. Owolabi).

https://doi.org/10.1016/j.gsd.2020.100531
Received 18 May 2020; Received in revised form 25 November 2020; Accepted 25 November 2020
Available online 1 December 2020

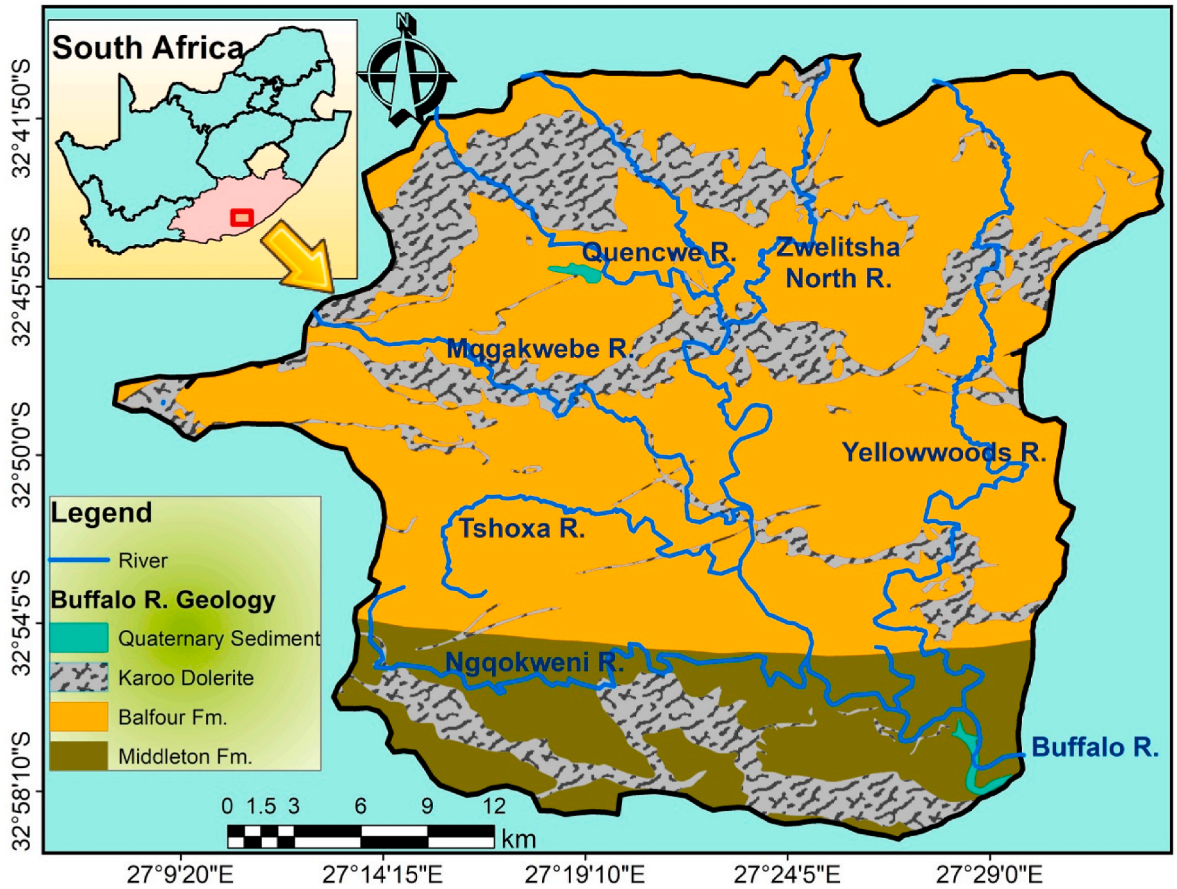

Fig. 1. Buffalo basin geology map showing the headwater drainage, and its lithostratigraphy.

areas of secondary porosity such as shear zones, trenches, elongated joints, major faults, and fractures, generally referred to as natural lineaments (Singhal and Gupta, 2010). Lineaments are tectonics structures developed by stress concentration or strains due to the initiation and evolution of rift and orogeny (Masoud and Koike, 2011). O'Leary et al. (1976) opined that they are extractible features of the earth with linear or curvilinear orientations on weak points of the earth's surface. They are often concentrated in areas with complex landforms (Galloway, 2010). They stretch over a few hundred meters to several kilometers on the surface and in the subsurface. Lineament mapping has a long history (Wilson, 1936; Moody and Hill, 1956; O'Leary et al., 1976). Lineaments can be processed and extracted manually or automatically from remotely sensed images, aeromagnetic data, and seismic lines (Madi and Zhao, 2013; Adiri et al., 2017; Baiyegunhi and Gwavava, 2017). Their application has gained wide recognition for groundwater prospecting (Nag, 2005), for the study of tectonic evolution (Boutirame et al., 2019), and mapping shear zones of ore mineralization (Eldosouky et al., 2020).

The precision of lineament detection depends on image enhancement tools such as the transformation computations, the enhancement filters, the algorithm efficiency, and the image quality or the extent of distortion. Randomness in nature and electromagnetic radiation interfere with image quality by raising the inherent noise level and producing outlying frequencies, morphological, and tonal variation which accounts for the distortion in the quality of the image. However, enhancement filters (such as convolution, Laplacian and Sobel filters, and Principal Component Analysis) serve as the tools for correcting the distortions (Sukumar et al., 2014). For further improvement of the aeromagnetic and gravity signal, transformation computation is applied to redefine the geophysical signal as a function with a finite length segment along a defined axis and for the alteration of the domain of the function. For example, Fast Fourier Transform works by redefining the square and periodic domain of a magnetic and gravity body to the wavenumber domain (Baiyegunhi and Gwavava, 2017).

In South Africa, large scale geologic structures within the Karoo Supergroup have been explored for their groundwater resources and shale gas potential (Chevallier and Woodford, 1999; Andreoli et al., 2006; Madi and Zhao, 2013; Baiyegunhi and Gwavava, 2017). The present study intends to present a holistic lithostratigraphy characterization that enables the delineation of groundwater capture zones in a complex environment.

The novelty of the study lies in the three-dimensional characterization of lithology for visualization of hydrostratigraphic domains based on the clustered approach of geomagnetism, geoinformatics, and sequence stratigraphy correlation. The following research questions were addressed:

1) Can the relationship between the swarms of lineaments and the tectonic stress field be deduced?
2) Do the geomorphic-based surficial lineaments have a significant relationship with magnetic and neotectonic structures?
3) How can a holistic three-dimensional configuration of the basement be evaluated?
4) What amount of groundwater information can be drawn from the inferred hydrostratigraphic units?

The clustered geophysics and geoinformatics methods present a catchment-based geologic assessment that is scoped into the following objectives: 1) to assess the geology of the environment through comparative analysis of geomagnetic imprint and sequence stratigraphy correlation; 2) to explore the interrelationship between the surficial lineaments, neotectonic structures, the subsurface lineaments, and the tectonic stress field; and 3) to infer hydrostratigraphic controls on

Table 1
Lithostratigraphy of beaufort group (Johnson et al., 2006).

GROUP (Supergroup)	SUBGROUP	FORMATION (Member)		LITHOLOGY	Thickness (m)	Epoch (period)	
				Alluvium, Dunes and beach sands	Varies	Holocene (Recent)	
BEAUFORT (Karoo)	**TARKASTAD**	Burgersdorp		Red Mudstone Sandstone Light Grey Sandstone Grey Shale	1000	Triassic	Anisian
		Katberg		Light Grey Sandstone Red Mudstone Grey Shale	900		Scythian
	ADELAIDE	**Balfour**	Palingkloof	Red Mudstone Light Grey Sandstone	50	Permian	Tatarian
			Elandsberg	Sandstone Siltstone	700		
			Barberskrans	Light Grey Sandstone Khaki Shale	100		
			Daggaboersnek	Grey Shale Sandstone Siltstone	1200		
			Oudeberg	Light Grey Sandstone Khaki Shale Grey & Black shale	100		Kazarian
		Middleton		Light Grey Sandstone Red Mudstone	1500		
		Koonap (Abrahamskraal)		Grey Sandstone Shale	1300		Ufimiam

groundwater prospects of the study area.

2. Study area description

The study was carried out in the Buffalo headwaters catchment. It is located within latitude 32°39′ to 33°05′ S and longitude 27°05′ to 27°33′ E, covering approximately 1237 km^2 (Fig. 1). It is drained by dendritic foothill drainage, comprising of six tributaries and the main stem of the Buffalo River which is 46 km long. It runs northwest-southeast from an altitude of approximately 1338 m in the Isidenge forest to the catchment mouth at Laing dam at an altitude of 267 m above sea level (Owolabi et al., 2020b). The foot slope is covered by colluvium and alluvial fan of about 2 m to 8 m thick in the valley bottom. The catchment soil maturity is quite low due to the shallowness of the underlying bedrock of clastic sedimentary materials and the crystalline basement (Owolabi et al., 2020a).

3. Geological setting and stratigraphy

The geology of Buffalo catchment comprises Tatarian red and grey mudstone of the Balfour Formation, covering three-quarters of the catchment. The lower quarter of the catchment grades into the older Kazarian silty-sandstone-dominated arenaceous strata of the Middleton Formation. The two formations fall within the Beaufort Group, Adelaide subgroup of the Karoo Supergroup (Baiyegunhi et al., 2017). The Balfour Formation has been noted to comprise five members, namely Oudeberg, Daggaboersnek, Barberskrans, Elandsberg, and Palingkloof Members (Katemaunzanga and Gunter, 2009). These were grouped into arenaceous and argillaceous units. The sedimentary facies of the catchment represent fluvio-deltaic alluvial deposits with lateral and downstream accretion in their flood paleochannel (Wilson et al., 2014). The catchment hydrostratigraphy is laterally bounded at the north and south by a Jurassic dolerite outcrop and interspersed in various sections by Jurassic dolerite dykes and sills. Lithostratigraphy of the Beaufort Group is presented in Table 1.

4. Materials and methods

An integrated geo-structural framework of digital processing of aeromagnetic data and Landsat 8 Operational Land Imager (OLI) was employed to characterize the hydrostratigraphy domain and to define the macroscale geologic structures of the geologic environment.

4.1. Geomagnetic analysis

The aeromagnetic data of Buffalo catchment was extracted from the regional aeromagnetic survey of Eastern Cape, mapped by Fugro Airborne Surveys for the Council for Geoscience. The aeromagnetic data mapping was achieved with the aid of a proton procession magnetometer of 0.01 nT resolution. The aeromagnetic scanner was flown at a constant height of 60 m in north-south flight direction, within a sampling line of 250 m using line spacing of 200 m.

4.1.1. The reduced-to-pole mapping

The aeromagnetic data was processed through linear and non-linear filtering algorithms of the Montaj MAGMAP filtering system. The space domain grid was prepared first. This enables the reduction of long wavelength and high amplitude behavior. It ensures an adequate gap for periodicity and maintains the power and frequency content in the data at the same level (Li and Oldenburg, 1998). The total magnetic field intensity (TMI) has a range of −44.1 to 52.6 nT. The average magnetic inclination of 63.4667° and declination of −28.6667° were applied after removing the International Geomagnetic Reference Field to plot a reduced-to-pole map (Peddie, 1982). The reduced-to-pole mapping enables the correction of total magnetization intensity for spatial distortion and removal of anomaly skewness while the data format and polarity are preserved (Guo et al., 2013). By so doing, the computation process enables the repositioning of the high magnetic amplitude vertically on the magnetic source (Baranov, 1957). This enables the delineation of the tectonic stress field induced by Jurassic dolerite sills and dykes at great depth. This was done by computing twice the differentiation of the source function in the vertical direction according to equation (1) (McKenzie et al., 2012). The first differentiation enables the deduction of magnetization potential corresponding to the vertical component of the magnetic source while the second differentiation enables the alignment of the magnetic anomaly in the vertical direction of the magnetic potential.

$$\Delta T_y(r) = \frac{\delta^2}{\delta y^2} \iint_{-\infty}^{\infty} \Delta T(r) \cdot \delta\rho \cdot \delta b \tag{1}$$

where $T_y(r)$ connotes the reduced-to-pole magnetic anomaly based on the vertical magnetization y, r is the radius of the magnetization field from the source to the observation, ρ is the direction of the uniform anomalous magnetization, and b is the direction of the Earth's main field.

4.1.2. Analytical signal mapping

A two-dimensional forward and inverse Fast Fourier Transform algorithm was applied to convolve and filter the data in the wavenumber domain. The analytical signal (AS) and the total horizontal derivatives of tilt derivatives (THDTDs) were computed for structural delineation of basement configuration. Principally, AS Transform convolves the magnetic amplitude from a magnetic inclination to a non-skewed magnetic signature, thus enabling the resultant and symmetrical positioning of a magnetic anomaly on its causative bodies (Nabighian, 1972; Pilkington and Keating, 2004). In this work, the need for a conceptualization of the hydrostratigraphy domain and contact zones of dolerite-host rock necessitates the mapping of AS. This was computed, based on equation (2) shown below:

$$AS(x,y,z)=\sqrt{\left(\frac{\Delta T_y(r)}{\delta x}\right)^2+\left(\frac{\Delta T_y(r)}{\delta y}\right)^2+\left(\frac{\Delta T_y(r)}{\delta z}\right)^2} \quad (2)$$

where $T_y(r)$ is the reduced-to-pole magnetic anomaly is the measured field, and x, y, and z are the edges of the magnetic structures.

4.1.3. Magnetic lineament detection

A THDTD was computed to delineate the effective position of the subsurface linear features such as fractures and faults (magnetic lineaments), which may influence the preferential flow-path of groundwater. The THDTD computation of the total magnetic intensity T is based on equations (3) and (4) shown below:

$$TDR=arctan\left(\frac{\frac{\delta T}{\delta z}}{\sqrt{\left(\frac{\delta T}{\delta x}\right)^2+\left(\frac{\delta T}{\delta y}\right)^2}}\right) \quad (3)$$

$$THDTD=\sqrt{\left(\frac{\delta TDR}{\delta x}\right)^2+\left(\frac{\delta TDR}{\delta y}\right)^2} \quad (4)$$

where T is the total magnetic intensity and TDR is the tilt derivative.

4.1.4. Assessment of depth of the magnetic source

The magnetic depth slicing was carried out using Getech GetGRID. The depth slicing linear filter computes the apparent depth to magnetic source as a plot of magnetic field gradients across the subsidence of magnetic anomaly. The computation procedure is based on Wiener filtering principle whereby the magnetic signal is assumed to be due to two or more invariant arbitrary processes (Baiyegunhi and Gwavava, 2017). The components of the magnetic gradient were extracted from the gradient plots by disaggregating the shallow sources from the deeper sources. This was done by fitting trend-lines to join the vertices of major tilts on the plot. The depth estimation is based on the slope of the fitted trendline as defined in equation (5):

$$h=\frac{b}{-4\pi} \quad (5)$$

where h is the average depth to the anomalous structure in meters and b is the slope of the Nyquist wavenumber components. The information on the derivation, manipulation, and general discussions of magnetic filtering techniques and equations projected above are documented in detail in Whitehead and Musselman (2008).

4.2. Auto-lineament detection

Secondly, surficial lineaments were processed using the panchromatic band of Landsat 8 OLI. The image selection for the Landsat 8 OLI imagery was based on less than 10% low cloud scene and critical visual inspection of the satellite image. Further atmospheric correction for noise removal, improvement of radiometric value, and pan-sharpening was carried out on the selected band, in PCI Geomatica software. The selection of the pan-chromatic band (Band 8) was because of its high spatial resolution (15 m). It is the only band whereby visible colors are integrated into a single channel (Amer et al., 2009).

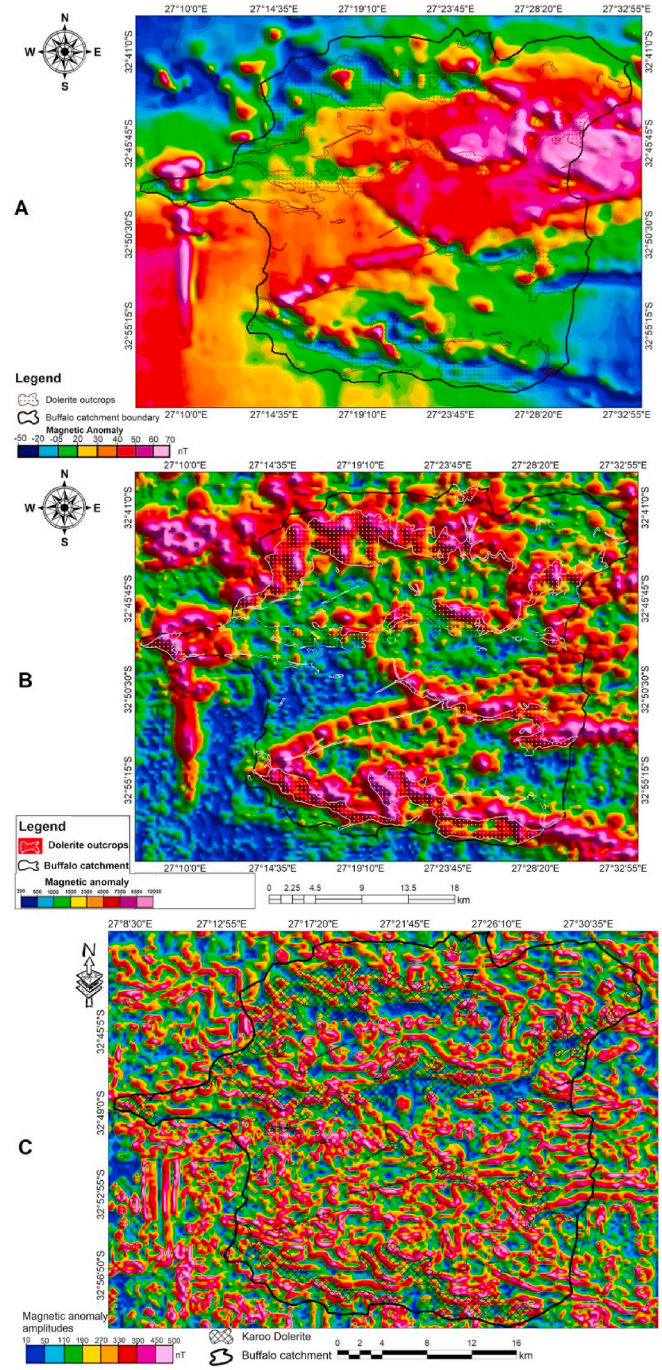

Fig. 2. a). RTP magnetization anomaly map indicating the geologic source of dolerite and the regions of low lithostatic stress at time of intrusion which coincides with the area of dolerite outcrop; b). Analytical signal map; the dolerite outcrop correlates with the areas of high nT magnetic anomaly, and; c). THDTD map of Buffalo basin.

The surficial lineaments were digitized through a multi-stage line detection algorithm of Canny edge and contour detection enhancement using PCI Geomatica, 2017 version. Curve detection was filtered using the contour detection enhancement. A four-stage line algorithm specifies the minimum length of a curve, the maximum error based on a line fitting threshold, the maximum angle between the polyline segments based on the angular difference threshold, and the minimum distance between two polylines based on the linking distance threshold (Hashim

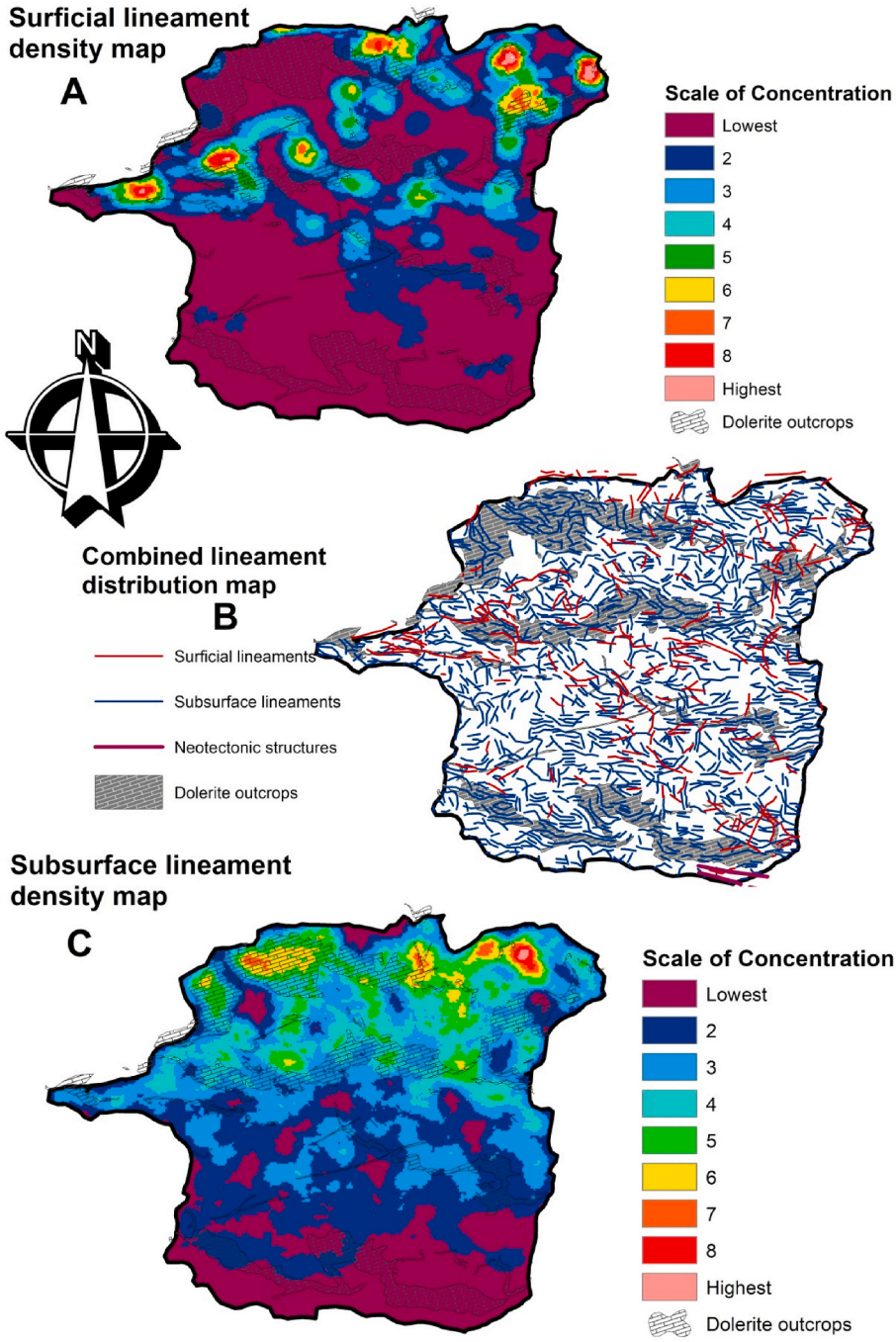

Fig. 3. Lineament distribution and lineament density map showing: a) surficial lineament density; b) the swarms of surficial and subsurface lineaments; C) subsurface lineament density.

et al., 2013). The statistical summary of the extracted lineaments was computed in ArcGIS 10.5.1. The information on the lineament angular direction was extracted by splitting the linear features at the vertices. The linear feature classes were plotted on a rose diagram in Rockworks 17. The linear features of the THDTD map were also extracted and computed for their azimuthal information. The lineament density for the surficial and magnetic lineaments was computed using ArcMap 10.5.1.

The deductions from the assessments were corroborated by a sequence stratigraphy correlation using borehole lithology data mapped in Strater 5. The borehole lithology data were acquired from the National Groundwater Archive of the Department of Water and Sanitation, South Africa. The field geologic survey involving sampling of sedimentary facies based on their detrital sizes, structural and textural attributes enabled the delineation of members of the Balfour Formation within the catchment. The extracted geologic information was compared with scanned soil composition and geomorphological map, to produce the sedimentary facies map.

5. Results

5.1. Tectonic stress field of the Jurassic dolerite

The reduction-to-pole (RTP) map (Fig. 2a) presents the spatial distribution of the tectonic stress whereby the areas of anomalous magnetic intensity typify the source of the remnant magnetization of the causative body. The RTP transformation removes dipolar attributes of magnetic

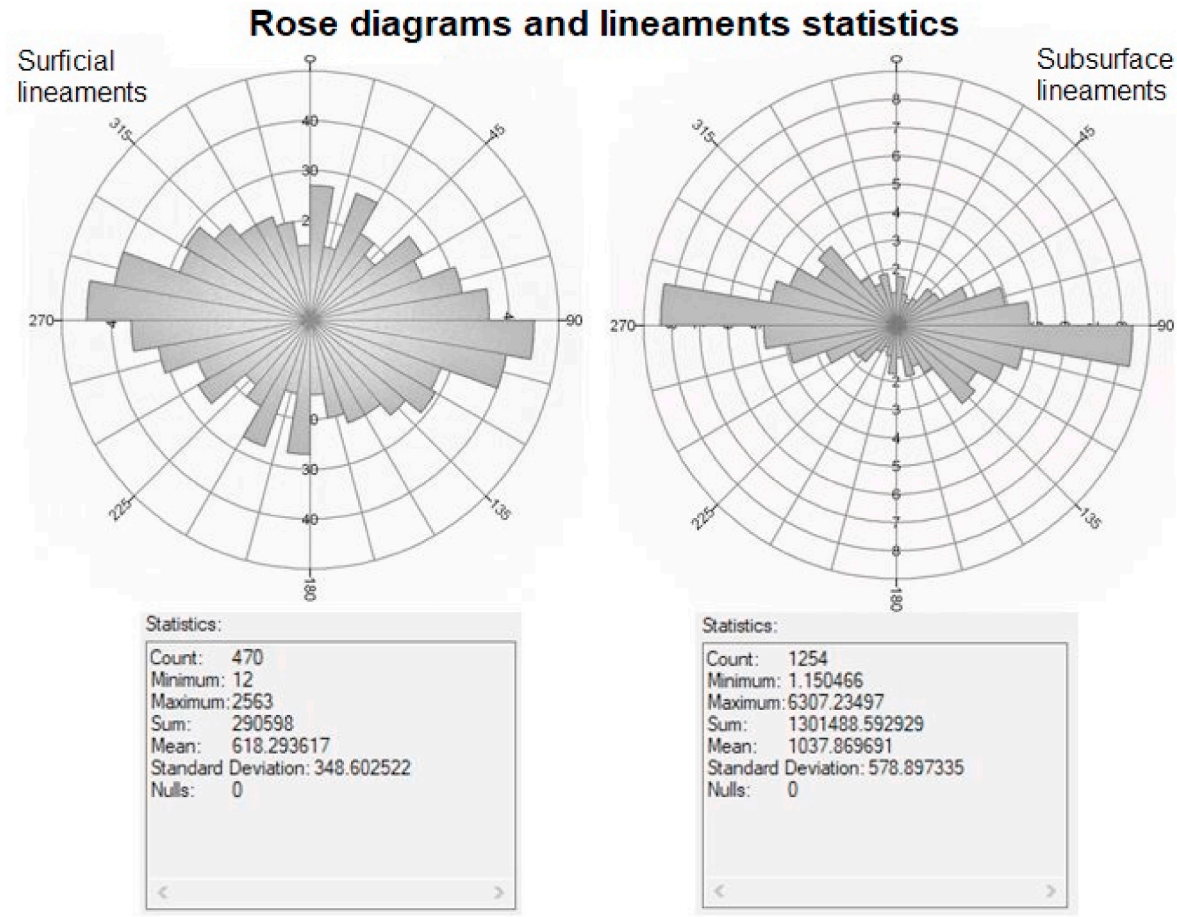

Fig. 4. Buffalo basin lineaments rose diagrams and their statistical information (in meters).

anomalies by reorienting the magnetic anomaly into a normalized and symmetrical pattern (Abedi et al., 2013). Hence, the anomalous sources of the remnant magnetization indicate the field of tectonic stress as shown at the northwest and other spots in the north, center, extreme west, southwest, and south. This assessment provides information on the source of crustal deformation and fracture system in the contact zones of dolerite intrusion and the country rock (Ingebritsen and Manning, 2003; Montanari et al., 2017). The lineaments produced by magnetic lows of the RTP transformation correlate visually with the areas of emplacement of the dolerite rocks.

5.2. Geomagnetic mapping of shallow dolerite

The AS transformation computes the magnetic signal by registering the crest of a magnetic anomaly within the borders of the magnetic bodies at shallow depth. Hence, the resulting map delineates the areas of emplacements of magnetic bodies in a manner that is independent of induced or remnant magnetization and magnetic inclination or declination (Fig. 2b). The high AS amplitude within the range of 6000–10,000 nT shows a significant spatial correlation with dolerite features especially the two dolerite dykes lying west-east at the north and the south of the study area. Moreover, the deductions helped in identifying the minor dolerite sills and dykes which were concealed by low-resolution mapping at a regional scale as well as the dolerite outcrop and near-surface features in inaccessible locations. The dolerite outcrops were estimated to cover 281 km^2 (22.72%) while the shallow dolerite intrusion, within the range of 4500 nT–6000 nT was estimated at 228 km^2 (18.46%). The possible hydrostratigraphic relevance of the intermediate AS amplitude (500–1500 nT) and the extremely low AS amplitude (0–250 nT) was further inspected. The amplitudes are due to the residual geomagnetic properties of the clay-rich argillaceous strata and of non-magnetic arenaceous strata (Vaniman et al., 2014; Vogel et al., 2015). The relationship between the position of the major dolerite outcrops and the RTP lineaments suggests that the magnetic lows of RTP are likely to constitute the synclinal area of the emplacement of geologic intrusion (Fig. 2a).

5.3. Lineaments distribution

The THDTD analysis enables the spatial configuration of magnetic relief and textures corresponding to the variation in magnetic susceptibility of host rock and subsurface fractures (Fig. 2c). The linear and curvilinear features of low-amplitude magnetic responses are truncated residual magnetization anomalies that are possibly linked with neotectonic movements (Middleton et al., 2015). The surficial lineaments extracted from the rectified panchromatic band of Landsat 8 OLI (Fig. 3b) show a high degree of correlation with the tectonic stress field presented by the RTP map. Most of the delineated magnetic lineaments trend WNW–ESE, the same direction as the surficial lineaments. The surficial and subsurface lineaments vary in length from 12 m to 2563 m and 1.15 m–6307 m, respectively (Fig. 4). The two sets of lineaments align with the neotectonic structural lineaments which also trends WNW–ESE in the extreme south of the catchment (Fig. 3). The radial trend-pattern of the surficial lineaments rose diagram depicts a combination of geomorphic alterations, crustal weak zones, shear zones, thrust and reverse faults. These are considered excellent pathways for groundwater flow. Similarly, the surficial lineaments exhibited a geospatial relationship with Buffalo drainage in a manner that indicates the

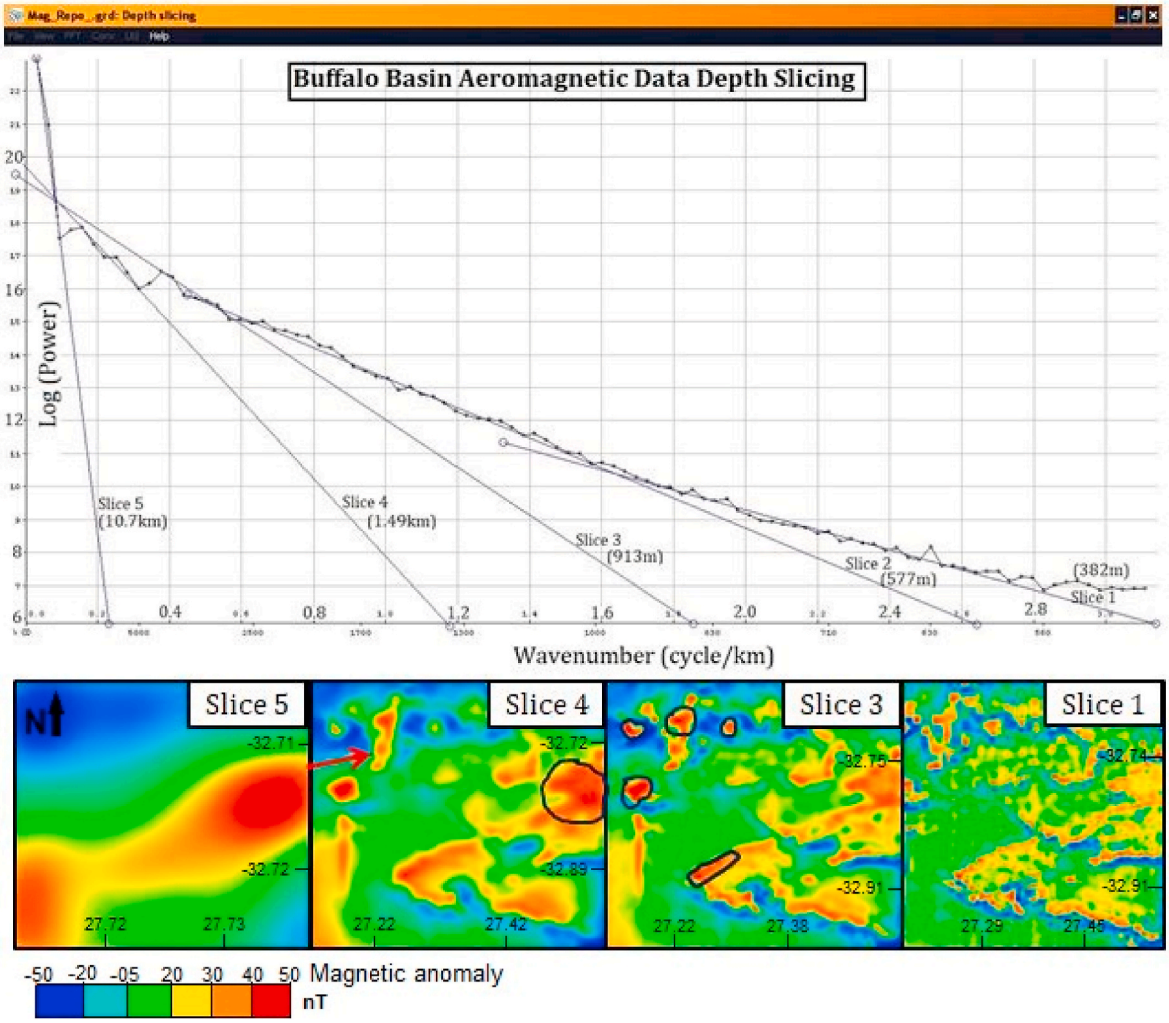

Fig. 5. Depth slicing; the corresponding effective anomaly is shown with a blue ring while the deepest (Slice 5) is shown with a red arrow. The red dots in Slice 1 reveal the effective anomaly corresponding to the dolerite geologic source at the estimated depth being sliced. (For interpretation of the references to color in this figure legend, the reader is referred to the Web version of this article.)

structural influence on the Buffalo River.

5.4. Depth assessment of tectonic stress field

The result of the magnetic source position based on a radially averaged power spectrum is presented in Fig. 5. The five major trend-lines extracted and lying at depths of 382 m, 577 m, 913 m, 1.49 km, and 10.7 km connote the trenches of a deep-seated tectonic stress field, identified as the sills and feeder dykes. Slice 1 suggests that most of the shallow dolerite intrusions are emplaced at 382 m depth, while the pattern is replicated in Slice 2, thus suggesting that the shallow geologic intrusions have a thickness of at least 195 m. Slice 3 (913 m), which is also replicated by slice 4 (1.49 km), presents much broader sills, believed to be the source for the shallow feeder dykes. The discernment of the dyke trenches based on the connection of the slices suggest that most of the geologic intrusion occurs in the W–E, WSW–ENE, and WNW–ESE directions. The deepest tectonic stress field lies at the depth of 10.7 km, shown at the northwest. This is presumably the tectonic source of the main W–E dyke at the north of the catchment and possibly accounts for the high density of subsurface and surface lineaments in the north as shown in Fig. 3a and c.

5.5. Validation of the geologic model

The south section of the catchment mapped as Daggaboersnek Member by Katemaunzanga and Gunter (2009) is characterized by non-lenticular argillaceous rock deposited by lateral and downstream accretion (Figs. 6 and 7a). The section grades into arenaceous rock with a flat-topped laminated sheet of sandstone and lateral accretionary mudstone deposit at the Ngwokweni headwaters. The Barberskrans Member is dominated by massive coarse yellow sandstone (Fig. 7b), subordinate siltstone, and red mudstone by the Mgqakwebe and Tshoxa river-cut in the west. The sandstone appears as a multi-story section with a flat-topped tabular platform in the east to the southeast along the Yellowwoods River (Fig. 7b). The Barberskrans Member grades into the Elandsberg Member, characterized by intercalated arenaceous rocks, enriched in shale and interspersed with silty sandstone along some sections of the Quencwe River at the northwest Pirie Fish farm. The Elandsberg Member is associated with crevasse channel ribbon complexes whose accretionary pattern is fluvio-deltaic. Towards the Rooikrans dam, the lamina deposit tapers into the Quaternary sediments. The Palingkloof Member is dominated by reddish-brown bedded mudstone formed as floodplain deposits.

The catchment geologic cover is characterized by weathered and densely fractured dolerite outcrops as well as detached dolerite boulders in the north. Towards the west and center of the catchment, the dolerite

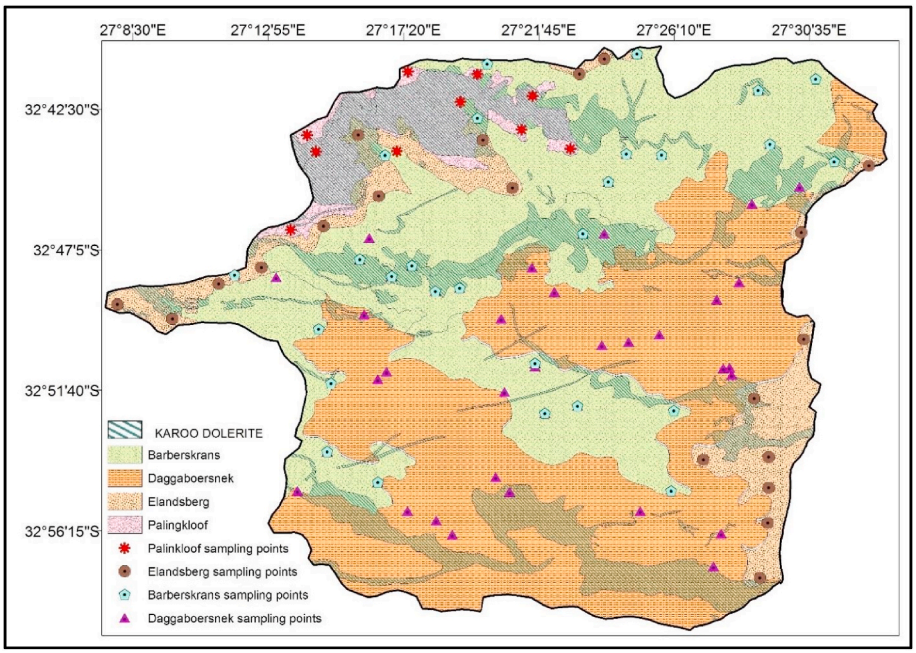

Fig. 6. Sedimentary facies map of Buffalo catchment. 10 Palinkloof sampling points, 20 sampling points of Elandsberg, 26 Barberskrans sampling points, and 27 Daggasboersnek sampling points.

surface is characterized by joints or solution holes due to weathering action. In the northwest, the dolerite spreads appear as pyroclastic round-top dykes amidst hilly landforms. The dolerite outcrops in the south are quite fresh with limited fractures, joints, or solution holes compared to those of the north. The argillaceous sections of the catchment show a moderate spatial correlation with the intermediate signals (500–1500 nT) obtained from the AS map. Also, the extremely low signals (0–250 nT) correlate with the arenaceous rocks of the Barberskrans Member, and this, as a result, presents the analytical signal model as an important imprint for hydrostratigraphic modeling.

The ramification suggested by AS amplitude disbandment was further examined through sequence stratigraphy correlation (SSC) of lithologic logs from 34 shallow boreholes, presented in Table 2 and Figs. 8 and 9. The SSC shows that the overburden of the northern half of the Buffalo basin is mostly characterized by mudstone and sandstone (QL, ML1, and YL1) while the southern half is mostly characterized by sandstone and shale (TL, ML2, NL1, NL2, and YL2) as indicated by the field survey report. The SSC also reveals the possible existence of a fault system in the northern profiles (QL, ML1, TL, and YL1) where the dolerite section pinches out unconformably against another. In a similar manner to the survey, the SSC corroborates the extremely low signal to be the sandstone-dominated units (F44, F88, F17, A2, and F26). Meanwhile, the intermediate signal is corroborated to be dominated by argillaceous sedimentary clast (F31, F20, F89, A6, C31, and C14) as shown in Fig. 8.

The three-dimensional projection of the total residual magnetization confirms that the northern half is associated with spikes of dolerite intrusion which possibly influence the development of the complex topographic system (Fig. 10). The tectonic stress induced by the geologic intrusion as indicated by Slices 4 and 5 (Fig. 6) may have accounted for the uplift in the northwest, and influenced the fracture systems within the area.

6. Discussion

6.1. Buffalo lithostratigraphic settings

The lithology of the Buffalo catchment has been characterized for its basement configuration and macrostructures using geomagnetic analysis. The study enables the visualization of the landscape evolution from the uplift initiated by the dolerite intrusion in the northwest of the catchment (Fig. 10). The landform produced in the northwest coincides with the continental hinterland associated with the Amatole-Swaziland Range. The range was reported to be initiated by intercontinental rifting during uplift (Wildman et al., 2016). The tectonic stress field in the Buffalo catchment is localized at depths of 382 m, 577 m, 913 m, 1.49 km, and 10.7 km. The dolerite lineaments are oriented in the E–W, WNW–ESE, and WSW–ENE directions. The tectonic activity impacted the north of the study area and influenced the development of swarms of subsurface and surface lineaments trending WNW–ESE. The azimuthal correlation between the surficial lineaments, the subsurface lineaments, and the neotectonic structures further corroborates the relevance of surficial lineaments to geologic studies. The finding here agrees with Senger et al. (2015) on the localization of fractures and faults at the contact between Southern Karoo dolerite dykes and the country rocks. The findings on the orientation of the lineaments align with the reports of Andreoli et al. (2006) and Madi and Zhao (2013) on the existence of structural lineaments trending NW–SE in the region with the aid of seismic exploration. Also, Chevallier and Woodford (1999) noted that the orientation of dolerite sills and dykes in the Karoo is important for inferring neotectonic fractures since the dolerites are emplaced within the neotectonic structures. This finding was confirmed in this study by the positive correlation between the low-amplitude tectonic stress field of RTP (Fig. 2a) and the magnetic anomaly of AS map (Fig. 2b).

Additionally, the multiple strata in the lithology of some boreholes in the east (A24, C25, and F07) and the southwest (F20 and F44) indicates the existence of heterolithic deposition in some part of the Buffalo basin (Fig. 9a and b). The bedding suggests a successive deposition typical of a straight and faster-moving flow. This implies that the paleohydrology of the Buffalo basin is characterized by high energy flow and turbulent fluvial style which develops accretionary structures. The bedding indicates that the geology of the Buffalo basin is complex. This finding aligns with Catuneanu and Elango (2001) and Katemaunzanga and Gunter (2009) who posited the fluvial style of the Buffalo paleoenvironment. The heterolithic bedding of the Buffalo catchment suggests the possibility for highly variable groundwater flow on account of the

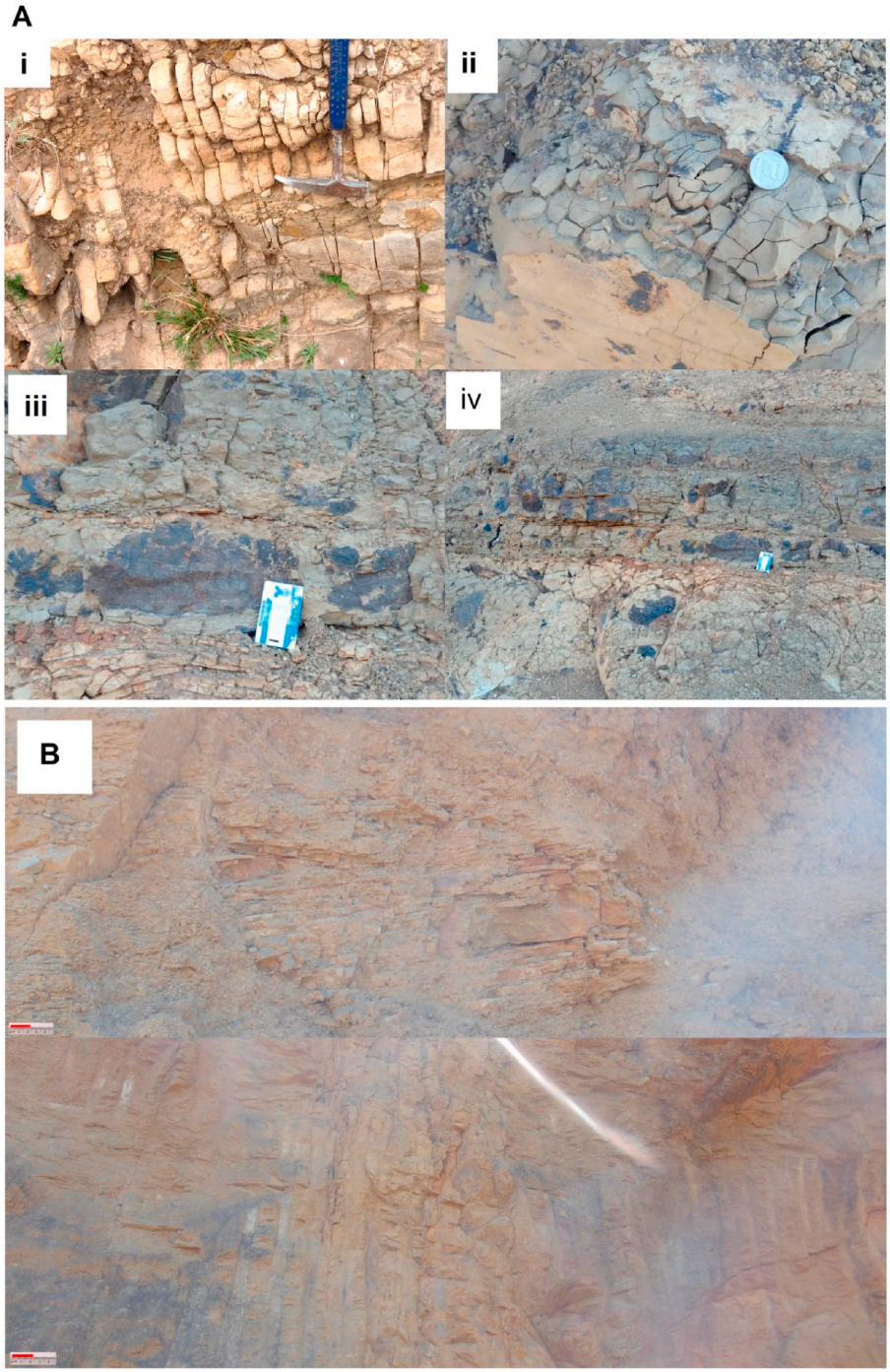

Fig. 7. a). Photograph of a Daggaboersnek Member showing (i) a section of weathered and jointed siltstone along a river cut, (ii) desiccation cracks of channel-filled grey mudstone, (iii) a weathered mudstone, and (iv) downward accretion of the mudstone shown in (iii), and; .b). Photograph of the Barberskrans Members showing coarse yellow sandstone. (For interpretation of the references to color in this figure legend, the reader is referred to the Web version of this article.)

varying hydraulic conductivity across the multiple lithologies.

An important finding in this study is the hydrostratigraphic characterization potential of AS disbandment. The correspondence between the intermediate amplitudes of the AS transform (500–1500 nT) and the argillaceous sedimentary rocks may be due to the residual magnetization of ferrihydrite, lepidocrocite, and goethite in the mudstone and shale (Islam et al., 2002; Vaniman et al., 2014; Vogel et al., 2015). Overall, the finding on the AS mapping conforms to the report of Baiyegunhi and Gwavava (2017) on the basement configuration of the study area within the southeastern Karoo.

6.2. *Delineation of Buffalo hydrostratigraphy for groundwater prospect*

The Buffalo basin is characterized by a fissured aquifer as the main hydrostratigraphic domain with a minor intergranular aquifer. The fissured aquifer of the Buffalo basin is localized in the north and influenced by the tectonic stress field where dolerite intrusion had contact with the host rocks as indicated by the lineament density maps (Fig. 3a and c; Owolabi et al., 2020c). The exposed dolerite and sandstone outcrops in the north are characterized by intense weathering and extensive joints and fractures in a way that aligns with the subsurface stress field. The fractured system in the basin is further confirmed by the existence of

Table 2
Table showing the few of the 134 borehole lithology drawn from 34 wells.

ID	Long	Lat.	DepthTop	Depth Bottom	Lithology	ID	Long	Lat.	DepthTop	Depth Bottom	Lithology
F31	−32.853	27.304	0	3.1	SOIL	A2	−32.950	27.283	1.2	45.7	Sandstone
F31	−32.853	27.304	3.1	45.7	Shale	F81	−32.943	27.284	0.0	1.0	SOIL
F44	−32.825	27.283	0	1.8	SOIL	F81	−32.943	27.284	1.0	15.0	Dolerite
F44	−32.825	27.283	1.8	91.4	Sandstone & Shale	F81	−32.943	27.284	15.0	48.7	Shale
F80	−32.821	27.281	0	1	SOIL	F83	−32.943	27.284	0.0	70.0	Sandstone
F80	−32.821	27.281	1	14	Dolerite	C34	−32.948	27.301	0.0	2.0	SOIL
F80	−32.821	27.281	14	61	Quartzite	C34	−32.948	27.301	2.0	25.0	Sandstone
F80	−32.821	27.281	61	75	Dolerite	C34	−32.948	27.301	25.0	30.0	Shale
F56	−32.827	27.265	0.0	3.6	Shale	C34	−32.948	27.301	30.0	72.0	Sandstone
F56	−32.827	27.265	3.6	87.0	Sandstone & Shale	F26	−32.910	27.370	0.0	2.0	SOIL
F58	−32.858	27.259	0.0	74.0	Sandstone & Shale	F26	−32.910	27.370	2.0	36.0	Sandstone
B03	−32.797	27.225	0.0	9.4	Shale	F26	−32.910	27.370	36.0	54.0	Shale
B03	−32.797	27.225	9.4	65.5	Dolerite	F26	−32.910	27.370	54.0	90.0	Dolerite
C11	−32.813	27.251	0.0	1.0	SOIL	F26	−32.910	27.370	90.0	141.5	Sandstone
C11	−32.813	27.251	1.0	6.0	Dolerite	F76	−32.919	27.400	0.0	15.5	Clay
C11	−32.813	27.251	6.0	21.0	Dolerite	F76	−32.919	27.400	15.5	52.0	Sandstone
C11	−32.813	27.251	21.0	22.0	Dolerite	F46	−32.917	27.396	0.0	75.0	Sandstone
C11	−32.813	27.251	22.0	54.0	Dolerite	C31	−32.766	27.348	0.0	0.8	SOIL
C11	−32.813	27.251	54.0	82.0	Shale	C31	−32.766	27.348	0.8	3.5	Clay
F80	−32.821	27.281	0.0	1.0	SOIL	C31	−32.766	27.348	3.5	25.3	Mudstone
F80	−32.821	27.281	1.0	14.0	Dolerite	C31	−32.766	27.348	25.3	118.0	Dolerite
F80	−32.821	27.281	14.0	61.0	Quartzite	F15	−32.763	27.360	0.0	1.5	SOIL
F80	−32.821	27.281	61.0	75.0	Dolerite	F15	−32.763	27.360	1.5	6.0	Clay
A6	−32.829	27.335	0.0	13.7	SOIL	F15	−32.763	27.360	6.0	100.0	Dolerite
A6	−32.829	27.335	13.7	50.9	Sandstone & Shale	C15	−32.766	27.366	0.0	1.3	SOIL
A6	−32.829	27.335	50.9	61.0	Sandstone	C15	−32.766	27.366	1.3	9.5	Clay
F89	−32.780	27.258	0.0	5.0	Clay	C15	−32.766	27.366	9.5	97.2	Dolerite
F89	−32.780	27.258	5.0	21.0	Dolerite	C15	−32.766	27.366	97.2	100.0	Mudstone
F89	−32.780	27.258	21.0	75.0	Shale	C14	−32.766	27.366	0.0	1.5	SOIL
F88	−32.780	27.258	0.0	74.0	Sandstone	C14	−32.766	27.366	1.5	48.3	Mudstone
F18	−32.788	27.313	0.0	2.0	SOIL	C14	−32.766	27.366	48.3	100.0	Dolerite
F18	−32.788	27.313	2.0	42.0	Dolerite	A24	−32.730	27.491	0.0	2.0	SOIL
F18	−32.788	27.313	42.0	60.0	Sandstone	A24	−32.730	27.491	2.0	3.0	Mudstone
F18	−32.788	27.313	60.0	84.0	Shale	A24	−32.730	27.491	3.0	9.0	Mudstone
F17	−32.800	27.308	0.0	3.0	SOIL	A24	−32.730	27.491	9.0	12.0	Mudstone

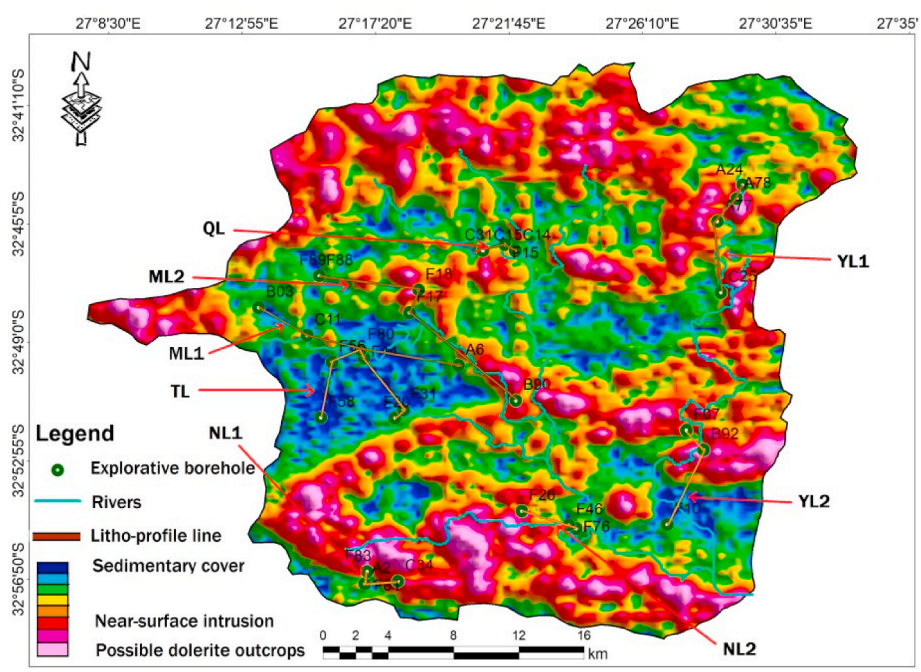

Fig. 8. Overlay of explorative boreholes on the analytical signal map for corroboration purpose.

quartzite lenses (A78 and F80; Fig. 9a and b). The clustered geomagnetic-lineament approach adopted here suggests that the creation of permeable contact zones between the Karoo dolerite dykes and the country rock depends on the complexity of the sedimentary layers (F26, F07, C25; Figs. 8, 9a and 9b). Hence, the fractured system produced by dolerite intrusions in the Buffalo basin is likely to vary in permeability as indicated by the lineament density map.

The main aquifer is expected to vary from low to moderate

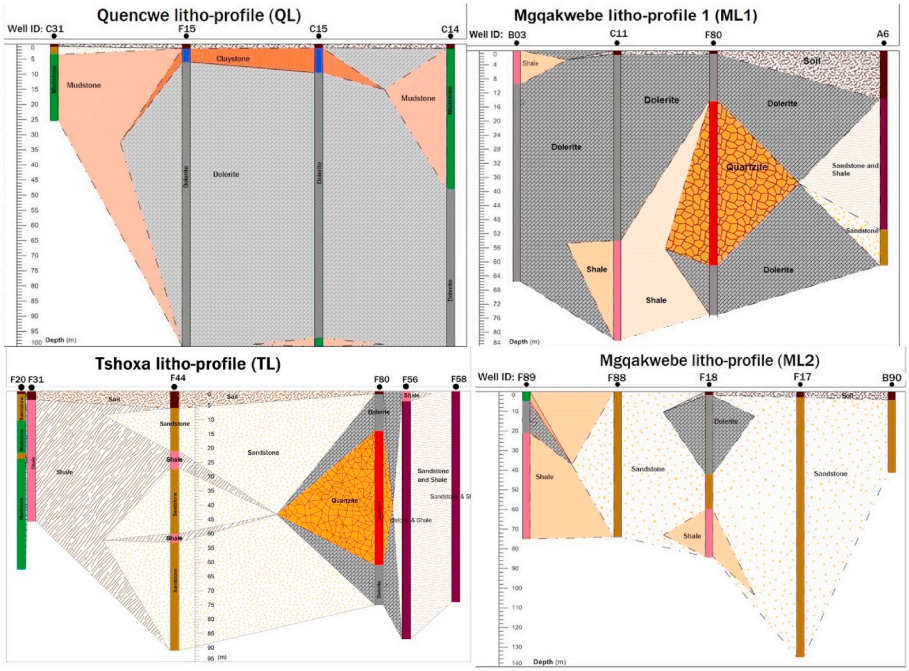

a: Borehole lithology cross-section profiles for north and west of Buffalo basin.

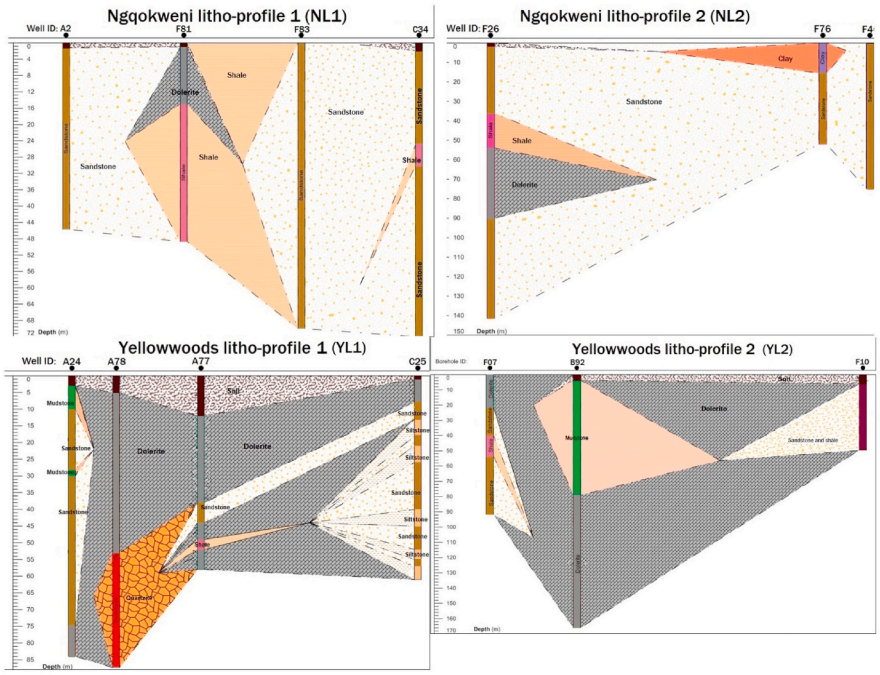

b: Borehole lithology cross-section profile for northeast, east, and south of Buffalo basin.

Fig. 9. a: Borehole lithology cross-section profiles for north and west of Buffalo basin. b: Borehole lithology cross-section profile for northeast, east, and south of Buffalo basin.

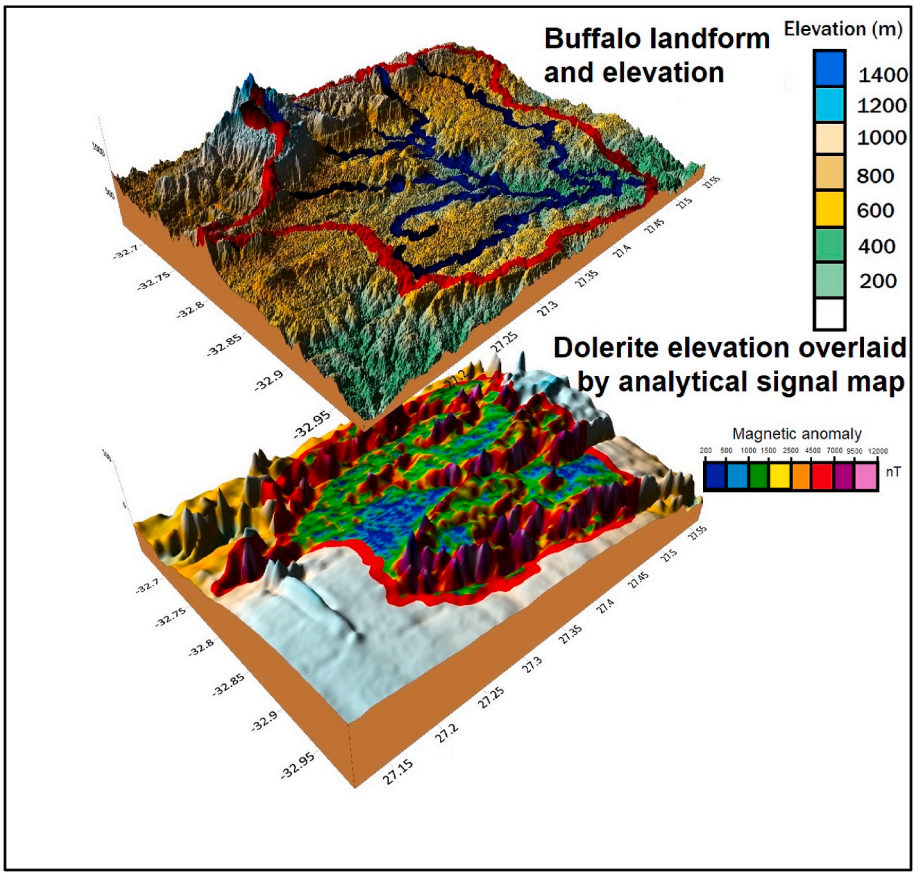

Fig. 10. Three-dimensional presentation of geomorphic configuration (DEM) and magnetic anomaly map (analytical signal on a total residual magnetic layer).

permeability and yield at the contact zone of dolerite and the host rocks in the Daggasboersnek and Barberskrans members, in agreement with Owolabi et al. (2020c; Fig. 6). Madi et al. (2016) also noted that the permeable contact zones of dolerite and country rock serve as an excellent conduit for groundwater flow. The variation in the contact zones is associated with the complexity of the sedimentary layers (F26, F07, C25; Figs. 8, 9a and 9b). DWA (2010) also posited that the catchment groundwater system is hosted by fractured and intergranular aquifers. The subordinate intergranular aquifer system in the Buffalo basin is possibly hosted in the sandstone within the Barberskrans Member (Fig. 6; Ramoeli, 2009). Further geophysical exploration may be required to ascertain the aquifer geometry.

Groundwater flow in the study area may be influenced by the WNW–ESE trends of the subsurface lineaments. The radial pattern of the surficial lineament cluster is significant for groundwater recharge where there is a high hydraulic head and discharge where the hydraulic head is lower. This discovery is instrumental for the protection of groundwater resources against pollution. Hence, the Department of Environment and the Department of Water and Sanitation are advised to work together to develop a policy to protect this area given the potential for land-use change. Agricultural activities such as fertilizer applications and industrial activities that generate chemical wastes are significant sources of groundwater pollutants in South Africa (Stevens and van Koppen, 2015). The vulnerability of water resources of the Buffalo catchment area to the effluent discharge from wastewater treatment plants and to chemical fertilizers have been reported by Chigor et al. (2013) and Okoh et al. (2015).

7. Conclusions

In this study, the regional groundwater prospect of the complex geologic environment was assessed using a clustered approach of aeromagnetic assessment, geoinformatics assessment, sequence stratigraphy correlation, and field survey. The following deductions were made:

- A conjunctive approach for lithostratigraphic analysis and its geologic structures provides holistic information on the hydrostratigraphic domain.
- The RTP map not only enables the identification of deep-seated geologic intrusion but also enables the modeling of tectonic impact on geologic terrain.
- The analytical signal proved to be a powerful reconnaissance tool based on variable sections of low magnetic amplitude that showed spatial correlation with argillaceous and arenaceous clasts.
- The authenticity of surficial lineaments as morphotectonic structures was demonstrated by their zonal and azimuthal correlation with subsurface lineaments and neotectonic structures.
- The study depicted that Buffalo basin geology is complex and heterogeneous. Any attempt to cross-correlate the lithologic data beyond 20 km will be pointless.
- The analysis enabled the characterization of Buffalo catchment as a fissured hydrostratigraphic domain with the shallow groundwater system hosted in the permeable contact zones of the dolerite and host rocks. The potential zones for the groundwater capture are the west, northwest, north, and northeast. However, further point exploration for groundwater depth is recommended.

The geoinformatics-geophysical approach for lithostratigraphic analysis is therefore recommended for adoption in areas with complex geology.

Declaration of competing interest

The authors declare that they have no known competing financial interests or personal relationships that could have appeared to influence the work reported in this paper.

Acknowledgments

We are grateful to Prof Ostwald Gwavava of the University of Fort Hare for his assistance with aeromagnetic data provision. Dr. (Ms.) Chinemerem Ohoro is thanked for her sacrificial support and assistance granted throughout the field geologic structure mapping.

Appendix A. Supplementary data

Supplementary data to this article can be found online at https://doi.org/10.1016/j.gsd.2020.100531.

References

Adiri, Z., El Harti, A., Jellouli, A., Lhissou, R., Maacha, L., Azmi, M., Zouhair, M., Bachaoui, E.M., 2017. Comparison of Landsat-8, ASTER and Sentinel 1 satellite remote sensing data in automatic lineaments extraction: a case study of Sidi Flah-Bouskour inlier, Moroccan Anti Atlas. Adv. Space Res. 60 (11), 2355–2367.
Abedi, M., Torabi, S.A., Norouzi, G.H., 2013. Application of fuzzy AHP method to integrate geophysical data in a prospect scale, a case study: seridune copper deposit. Boll. Geofis. Teor. Appl. 54 (2).
Amer, R., Kusky, T., Reinert, P.C., Ghulam, A., 2009. Image processing and analysis using Landsat ETM+ imagery for lithological mapping at Fawakhir, central-eastern desert of Egypt. In: ASPRS 2009 Annual Conference, Baltimore, Maryland.
Andreoli, M.A., Hart, R.J., Ashwal, L.D., Coetzee, H., 2006. Correlations between U, Th content and metamorphic grade in the western Namaqualand Belt, South Africa, with implications for radioactive heating of the crust. J. Petrol. 47 (6), 1095–1118.
Baiyegunhi, C., Gwavava, O., 2017. Magnetic investigation and 2½ D gravity profile modelling across the Beattie magnetic anomaly in the southeastern Karoo Basin, South Africa. Acta Geophys. 65 (1), 119–138.
Baiyegunhi, C., Liu, K., Gwavava, O., 2017. Sedimentation rate and subsidence history of the southeastern Karoo Basin, South Africa, using 1D backstripping method. Arab. J. Geosci. 10 (10), 225.
Baranov, V., 1957. A new method for interpretation of aeromagnetic maps: pseudo-gravimetric anomalies. Geophysics 22, 359–383.
Bense, V., van Balen, R., 2003. Hydrogeological aspects of fault zones on various scales in the Roer Valley Rift System. J. Geochem. Explor. 78, 317–320.
Boutirame, I., Boukdir, A., Akhssas, A., Manar, A., 2019. Geological structures mapping using aeromagnetic prospecting and remote sensing data in the karstic massif of Beni Mellal Atlas, Morocco. Maden Tetkik ve Arama Dergisi 160 (160), 1–10.
Catuneanu, O., Elango, H.N., 2001. Tectonic control on fluvial styles: the Balfour Formation of the Karoo basin, South Africa. Sediment. Geol. 140 (3), 291–313.
Chevallier, L., Woodford, A., 1999. Morpho-tectonics and mechanism of emplacement of the dolerite rings and sills of the western Karoo, South Africa. S. Afr. J. Geol. 102 (1), 43–54.
Chigor, V.N., Sibanda, T., Okoh, A.I., 2013. Variations in the physicochemical characteristics of the Buffalo River in the eastern Cape province of South Africa. Environ. Monit. Assess. 185 (10), 8733–8747.
Christensen, N.K., Minsley, B.J., Christensen, S., 2017. Generation of 3-D hydrostratigraphic zones from dense airborne electromagnetic data to assess groundwater model prediction error. Water Resour. Res. 53 (2), 1019–1038.
DWA (Department of Water Affairs), Groundwater Strategy 2010. Department of Water Affairs, South Africa.
Eldosouky, A.M., Sehsah, H., Elkhateeb, S.O., Pour, A.B., 2020. Integrating aeromagnetic data and Landsat-8 imagery for detection of accretionary shear zones controlling hydrothermal alterations: the Allaqi-Heiani Suture zone, South Eastern Desert, Egypt. Adv. Space Res. 65 (3), 1008–1024.
Galloway, D.L., 2010. The complex future of hydrogeology. Hydrogeol. J. 18 (4), 807–810.
Guo, L.H., Shi, L., Meng, X.H., 2013. The antisymmetric factor method for magnetic reduction to the pole at low latitudes. J. Appl. Geophys. 92, 103–109.
Hashim, M., Ahmad, S., Johari, M.A.M., Pour, A.B., 2013. Automatic lineament extraction in a heavily vegetated region using Landsat Enhanced Thematic Mapper (ETM+) imagery. Adv. Space Res. 51 (5), 874–890.
Ingebritsen, S.E., Manning, C.E., 2003. Implications of crustal permeability for fluid movement between terrestrial fluid reservoirs. J. Geochem. Explor. 78, 1–6.
Islam, M.R., Stuart, R., Risto, A., Vesa, P., 2002. Mineralogical changes during intense chemical weathering of sedimentary rocks in Bangladesh. J. Asian Earth Sci. 20 (8), 889–901.
Katemaunzanga, D., Gunter, C.J., 2009. Lithostratigraphy, sedimentology, and provenance of the Balfour Formation (Beaufort Group) in the Fort beaufort–alice area, eastern Cape province, South Africa. Acta Geol. Sin-Engl. 83 (5), 902–916.
Li, Y., Oldenburg, D.W., 1998. Separation of regional and residual magnetic field data. Geophys 63 (2), 431–439.
Madi, K., Zhao, B., 2013. Neotectonic belts, remote sensing, and groundwater potentials in the Eastern Cape Province, South Africa. Int. J. Water Resour. Environ. Eng. 5 (6), 332–350.
Madi, K., Nyabeze, P.K., Gwavava, O., Sekiba, M., Zhao, B., 2016. Magnetic and electromagnetic signatures around Polile Tshisa hot spring in the northern neotectonic belt in the Eastern Cape Province, South Africa. Acta Geophys. 64 (4), 943–962.
Marker, P.A., Foged, N., He, X., Christiansen, A.V., Refsgaard, J.C., Auken, E., Bauer, P., 2015. Performance evaluation of groundwater model hydrostratigraphy from airborne electromagnetic data and lithological borehole logs. Hydrol. Earth Syst. Sci. 19, 3875–3890.
Masoud, A.A., Koike, K., 2011. Auto-detection and integration of tectonically significant lineaments from SRTM DEM and remotely-sensed geophysical data. ISPRS J. Photogramm. 66 (6), 818–832.
McKenzie, B., Hillan, D., Foss, C., 2012. An improved search for magnetization direction. ASEG Extended Abstracts 1, 1–4.
Middleton, M., Schnur, T., Sorjonen-Ward, P., Hyvönen, E., 2015. Geological lineament interpretation using the object-based image analysis approach: results of semi-automated analyses versus visual interpretation. Geol. Survey of Finland, Special Paper 57, 135–154.
Montanari, D., Bonini, M., Corti, G., Agostini, A., Del Ventisette, C., 2017. Forced folding above shallow magma intrusions: insights on supercritical fluid flow from analogue modelling. J. Volcanol. Geoth. Res. 345, 67–80.
Moody, J.D., Hill, M.J., 1956. Wrench-fault tectonics. Geol. Soc. Am. Bull. 67 (9), 1207–1246.
Nabighian, M.N., 1972. The analytic signal of two-dimensional magnetic bodies with polygonal cross-section - its properties and use for automated anomaly interpretation. Geophysics 37, 507–517.
Nag, S.K., 2005. Application of lineament density and hydrogeomorphology to delineate groundwater potential zones of Baghmundi block in Purulia district, West Bengal. J. Indian Soc. Remot. 33 (4), 521.
Okoh, A.I., Sibanda, T., Nongogo, V., Adefisoye, M., Olayemi, O.O., Nontongana, N., 2015. Prevalence and characterisation of non-cholerae Vibrio spp. in final effluents of wastewater treatment facilities in two districts of the Eastern Cape Province of South Africa: implications for public health. Environ. Sci. Pollut. Res. 22 (3), 2008–2017.
O'Leary, D.W., Friedman, J.D., Pohn, H.A., 1976. Lineament, linear, lineation: some proposed new standards for old terms. Geol. Soc. Am. Bull. 87 (10), 1463–1469.
Owolabi, S.T., Madi, K., Kalumba, A.M., 2020b. Comparative evaluation of spatio-temporal attributes of precipitation and streamflow in Buffalo and Tyume catchments, Eastern Cape, South Africa. Environ. Dev. Sustain. 1–16.
Owolabi, S.T., Madi, K., Kalumba, A.M., Alemaw, B.F., 2020a. Assessment of recession flow variability and the surficial lithology impact: a case study of Buffalo River catchment, Eastern Cape, South Africa. Environ. Earth Sci. 77 (187).
Owolabi, S.T., Madi, K., Kalumba, A.M., Orimoloye, I.R., 2020c. A groundwater potential zone mapping approach for semi-arid environments using remote sensing (RS), geographic information system (GIS), and analytical hierarchical process (AHP) techniques: a case study of Buffalo catchment, Eastern Cape, South Africa. Arab. J. Geosci. 13 (22), 1–17.
Peddie, N.W., 1982. International geomagnetic reference field. J. Geomagn. Geoelectr. 34 (6), 309–326.
Pilkington, M., Keating, P., 2004. Contact mapping of gridded magnetic data – a comparison of techniques. Explor. Geophys. 35, 306–311.
Ramoeli, P., 2009. Explanatory Brochure for the South African Development Community (SADC). Hydrogeological Map & Atlas.
Senger, K., Buckley, S., Chevallier, L., Fagreng, Å., Galland, O., Kurz, T.K.O., Planke, S., Tveranger, J., 2015. Fracturing of doleritic intrusions and associated contact zones: insights from the Eastern Cape, South Africa. J. Afr. Earth Sci. 102, 70–85.
Singhal, B.B.S., Gupta, R.P., 2010. Applied Hydrogeology of Fractured Rocks. Springer Science & Business Media.
Stevens, J., van Koppen, B., 2015. Trends and Outlook: Agricultural Water Management in Southern Africa. Country Report – South Africa. Project Report Submitted to United States Agency for Int. Development's (USAID's) Feed the Future Program.
Sukumar, M., Venkatesan, N., Nelson, K.B.C., 2014. A review of various lineament detection techniques for high-resolution satellite images. Int. J. Adv. Res. Comput. Sci. Software Eng. 4 (3), 72–78.
Vaniman, D.T., Bish, D.L., Ming, D.W., Bristow, T.F., Morris, R.V., Blake, D.F., Chipera, S. J., Morrison, S.M., Treiman, A.H., Rampe, E.B., Rice, M., 2014. Mineralogy of a mudstone at yellowknife bay, gale crater. Mars Science 343 (6169).
Vogel, R.M., Lall, U., Cai, X., Rajagopalan, B., Weiskel, P.K., Hooper, R.P., Matalas, N.C., 2015. Hydrology: the interdisciplinary science of water. Water Resour. Res. 51 (6), 4409–4430.
Whitehead, N., Musselman, C., 2008. In: Montaj Grav/mag Interpretation: Processing, Analysis, and Visualization System for 3D Inversion of Potential Field Data for Oasis Montaj V6. 3, 85 Richmond. Geosoft Incorporated, St. W., Toronto, Ontario, M5H 2C9, Canada.
Wildman, M., Brown, R., Beucher, R., Persano, C., Stuart, F., Gallagher, K., Schwanethal, J., Carter, A., 2016. The chronology and tectonic style of landscape evolution along the elevated Atlantic continental margin of South Africa resolved by joint apatite fission track and (U Th Sm)/He thermochronology. Tectonics 35 (3), 511–545.
Wilson Jr., C.W., 1936. Geology of nye-bowler lineament, stillwater and carbon counties, Montana. AAPG Bull. 20 (9), 1161–1188.
Wilson, A., Flint, S., Payenberg, T., Tohver, E., Lanci, L., 2014. Architectural styles and sedimentology of the fluvial lower Beaufort Group, Karoo basin, South Africa. J. Sediment. Res. 84 (4), 326–348.